Turkish Journal of Chemistry

http://journals.tubitak.gov.tr/chem/

Research Article

Turk J Chem
(2019) 43: 809 – 824
© TÜBİTAK
doi:10.3906/kim-1811-55

Comparative study on physicochemical and mechanical characterization of new nanocarbon-based hydroxyapatite nanocomposites

Réka BARABÁS[1], Dennis DEEMTER[2], Gabriel KATONA[1], Gabriel BATIN[3], László BARABÁS[4], Liliana BIZO[5], Oana CADAR[6,*]

[1]Department of Chemistry and Chemical Engineering of Hungarian Line of Study, Faculty of Chemistry and Chemical Engineering, Babeş Bolyai University Cluj-Napoca, Cluj-Napoca, Romania
[2]University of Applied Sciences, Hochschule Osnabruck, Osnabruck, Germany
[3]Department of Materials Science and Engineering, Faculty of Materials and Environmental Engineering, Technical University of Cluj-Napoca, Cluj-Napoca, Romania
[4]Faculty of Mathematics and Computer Science, Babes-Bolyai University, Cluj-Napoca, Romania
[5]Department of Chemical Engineering, Faculty of Chemistry and Chemical Engineering, Babes-Bolyai University, Cluj-Napoca, Romania
[6]INCDO-INOE 2000, Research Institute for Analytical Instrumentation, Cluj-Napoca, Romania

Received: 26.11.2018 • **Accepted/Published Online:** 27.02.2019 • **Final Version:** 11.06.2019

Abstract: This study evaluated the effect of different additives such as nanocarbon compounds (0.5, 1.0, and 2.0 wt.%) with different morphologies and gelatin (Gel) (10 wt.%) on the mechanical properties of hydroxyapatite (Hap)-based nanocomposites (NCs). The NCs were prepared using the innovation process "SmartBox" based on the Internet of things (IoT), which provides process control and reproducibility, and they were characterized by X-ray diffraction, particle size distribution, transmission electron microscopy, Fourier transform infrared spectroscopy, and thermal analysis. The compressive strength tests demonstrated that the use of grapheme oxide (Hap_GO_2.0 - 133 N/mm^2), and/or Gel (Hap_Gel - 152 N/mm^2) as additives to reinforce Hap (106 N/mm^2) is more appropriate than the use of single functionalized multiwalled carbon nanotubes (Hap_fMWCNT_1.0 - 110 N/mm^2) and fullerene (Hap_Ful_0.5 - 106 N/mm^2).

Key words: Nanocarbon, gelatin, additives, hydroxyapatite, mechanical properties

1. Introduction

Hydroxyapatite (Hap) has chemical and crystallographic similarities to the natural inorganic components found in the bone matrix and teeth, offering good biological features such as biocompatibility, bioactivity, and osteoconductivity.[1,2] In addition to its high surface area, nano-Hap provides important host tissue interactions influencing osteoblasts adhesion and proliferation to improve tissue regeneration. However, one primary limitation is its poor mechanical properties, such as low fracture toughness and strength, and poor wear resistance.[3–6] To address this problem, specific reinforcing materials (carbon nanotubes, polyethylene, Al_2O_3, TiO_2, ZrO_2, etc.) are typically used to prepare Hap composites with enhanced mechanical properties; however, these materials exhibit bioactivity significantly lower than that of pure Hap.[7–9]

*Correspondence: oana.cadar@icia.ro

The reinforcing phases are either bioinert or considerably less bioactive, providing weak composite ability to form a stable interface with bone compared to pure Hap. Consequently, the ideal reinforcement material should significantly enhance the mechanical integrity with a low content of second phase.[10] Due to their excellent biocompatibility and mechanical properties, nanocarbon-based materials including zero-dimensional (0D) fullerene (Ful), one-dimensional (1D) carbon nanotubes (CNTs), two-dimensional (2D) layers of graphene, graphene oxide (GO), and reduced graphene oxide (rGO) are promising candidates for the reinforcement of biomaterial matrices.[11−13] Their properties are governed by their size, morphology, and structure. Therefore, the controlled synthesis of nanocarbons is the key to handling and tailoring their characteristics and widens their applications. Among these reinforcements, CNTs, especially multiwalled carbon nanotubes (MWCNTs), with their excellent stiffness and strength, have great potential to be used as a reinforcing agent for Hap without offsetting its bioactivity. The reinforcement of ceramics or polymer matrices with CNTs considerably enhances the structural properties such as fracture toughness, strength, elastic modulus, and wear resistance without affecting the properties of the reinforced material.[4−6] However, their biological safety with regard to toxicity issues, when considering the clinical applications of CNTs as biomaterials, is still controversial.[3,7]

The combination of organic and inorganic components allows materials with excellent biocompatibility and osteoconductivity to be obtained; in bone tissue, calcium phosphates are successfully combined with collagen fibrils. Natural polymers such as gelatin (Gel), chitosan, alginate, collagen, and starch-based materials are commonly used to produce high-quality Hap for biomedical applications.[14,15] Composite materials like Hap/collagen are of special interest in bone defect repair.[16] Gel, a product of partial collagen hydrolysis, exhibits attractive properties such as stability, less antigenicity than collagen, plasticity, adhesiveness, low cost, full resorbability in vivo, biocompatibility, and biodegradability, and its physicochemical properties can be suitably modulated.[17] However, the effects of Gel on Hap crystal morphology, mechanical strength, and biocompatibility are still not understood.[14]

The Internet of things (IoT) focuses on the interconnection and effective networking of machines and computing devices through the infrastructure of the Internet.[18] From a chemistry perspective, IoT improves the monitoring and control of a method's parameters, and relegates time-consuming data analysis and collection tasks to machines, leading to increased productivity, control, reproducibility, safety, and flexibility.[19]

For applications as potential bone replacement material, to mimic the real bone tissues it is important to develop composites with excellent mechanical and biological properties. Furthermore, the morphology control of nanocarbon-based nanocomposites (NCs) is critical to the application range because their physical and chemical properties are highly shape-dependent. Therefore, the aim of the present study was to examine the physicochemical and mechanical properties of Hap-based NCs using Gel and nanocarbon compounds with different morphologies (GO, functionalized multiwalled carbon nanotubes (fMWCNTs), and Ful) and amounts (0.5, 1.0, and 2.0 wt.%) to reinforce nano-Hap powders to overcome its poor mechanical strength in order to attain NCs with improved mechanical and biological performance.

2. Results and discussion

2.1. Laser diffraction particle size

The particle size analysis revealed an average particle size of 15 nm and no difference between the pure Hap and Hap-based NCs.

2.2. Morphology of Hap-based NCs

The morphology of Hap-based NCs was investigated by TEM (Figure 1).

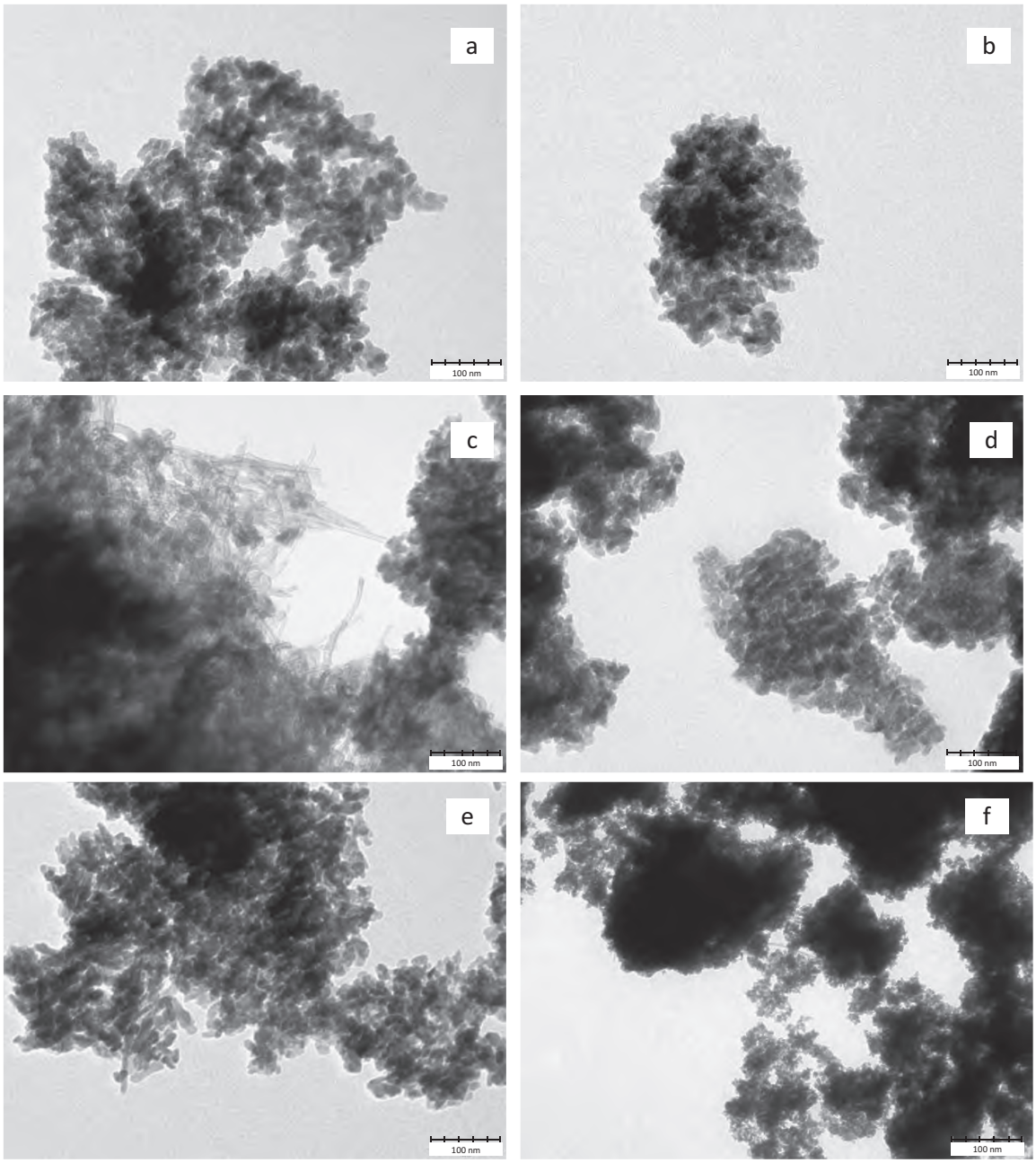

Figure 1. TEM images of (a) Hap, (b) Hap_Gel, (c) Hap_fMWCNT_1.0, (d) Hap_Gel_fMWCNT_1.0, (e) Hap_Ful_1.0, (f) Hap_Gel_Ful_1.0.

In all NCs, the nanocarbon additives showed good dispersion. The particles exhibited spherical shape morphology with an average size of about 10–20 nm. Furthermore, the particles in NCs containing Gel were rounder than those in NCs without Gel, suggesting a strong influence of Gel on particle morphology (Figures 1a and 1b).[20]

The growth of Hap nanoparticles on the CNTs indicated the formation of strong chemical bonds between them (Figures 1c and 1d). No CNTs were observed in the Hap_fMWCNT_Gel NCs, indicating full integration into the Hap nanoparticles, which is promoted by Gel. No traces of Ful were observed; a possible explanation could be the small size of the nanocarbon additives and their full integration into the Hap nanoparticles (Figures 1e and 1f).

2.3. XRD measurements

The XRD patterns of Hap and Hap-based NCs (Figure 2) exhibited only the characteristic diffraction lines of pure Hap (JCPDS file No. 09-0432). No significant differences were observed between the XRD patterns, suggesting a well-crystallized Hap (60%–68% crystallinity degree) deposited on the surface of the nanocarbon additives (CNT, Ful, and GO) and no obvious influence of Gel on the crystallization of Hap.[21] The average crystallite size (24–30 nm), estimated using the Debye–Scherrer equation, is presented in Table 1.

Table 1. Degree of crystallinity and crystallite size of Hap-based NCs.

NCs	Degree of crystallinity (%)	Crystallite size (nm)	NCs	Degree of crystallinity (%)	Crystallite size (nm)
Pure Hap	67.5	27.9	Hap_Ful_0.5	60.8	25.7
Hap_Gel	59.7	30.2	Hap_Ful_1.0	60.4	30.0
Hap_fMWCNT_0.5	63.3	29.5	Hap_Ful_2.0	58.6	25.3
Hap_fMWCNT_1.0	62.8	25.0	Hap_Gel_Ful_0.5	64.2	28.8
Hap_fMWCNT_2.0	65.6	29.3	Hap_Gel_Ful_1.0	45.6	26.9
Hap_Gel_fMWCNT_0.5	60.0	27.0	Hap_Gel_Ful_2.0	61.2	25.8
Hap_Gel_fMWCNT_1.0	56.8	24.9	Hap_GO_0.5	62.5	26.6
Hap_Gel_fMWCNT_2.0	55.4	23.7	Hap_GO_1.0	61.0	28.2
			Hap_GO_2.0	58.2	29.3

The characteristic peak of CNTs ($2\theta = 26.38°$) made no contribution to the specific peak of Hap ($2\theta = 25.84°$), indicating that peaks corresponding to the addition of CNTs did not appear. Similar to other studies, the XRD spectra of Hap and Hap-based NCs indicated no new phase or impurity.[6]

2.4. FT-IR analysis

The FT-IR spectra of Hap-based NCs containing 2 wt.% nanocarbon additives (fMWCNTs, Ful, and GO) are presented in Figure 3.

The FT-IR spectra of all NCs exhibited the characteristic bands of Hap (Figure 3a): the absorption bands of CO_3^{2-} (1420 and 875 cm^{-1}), PO_4^{3-} group (1036, 962, and 604 cm^{-1}), and adsorbed water (1600–1700 and 3200–3600 cm^{-1}).[22]

The FT-IR spectrum of Hap_Gel exhibited the bands assigned to C=O, C=C, and C–H stretching, bending, and scissoring vibrations of Gel (Figure 3b).[23] Similar to Hap_Gel, the bands at 1400–1750 cm^{-1} indicated the presence of Gel (C=O, C=C, and C–H stretching, bending, and scissoring vibrations).[24]

Beside the characteristic bands of pure Hap, the FT-IR spectra of Hap_fMWCNT_2.0 exhibited twin bands at 1028 and 1053 cm^{-1} attributed to the aliphatic P–O–C stretching (Figure 3c).[25] A similar FT-IR spectrum was observed for Hap_Gel_fMWCNT_2.0 (Figure 3d).

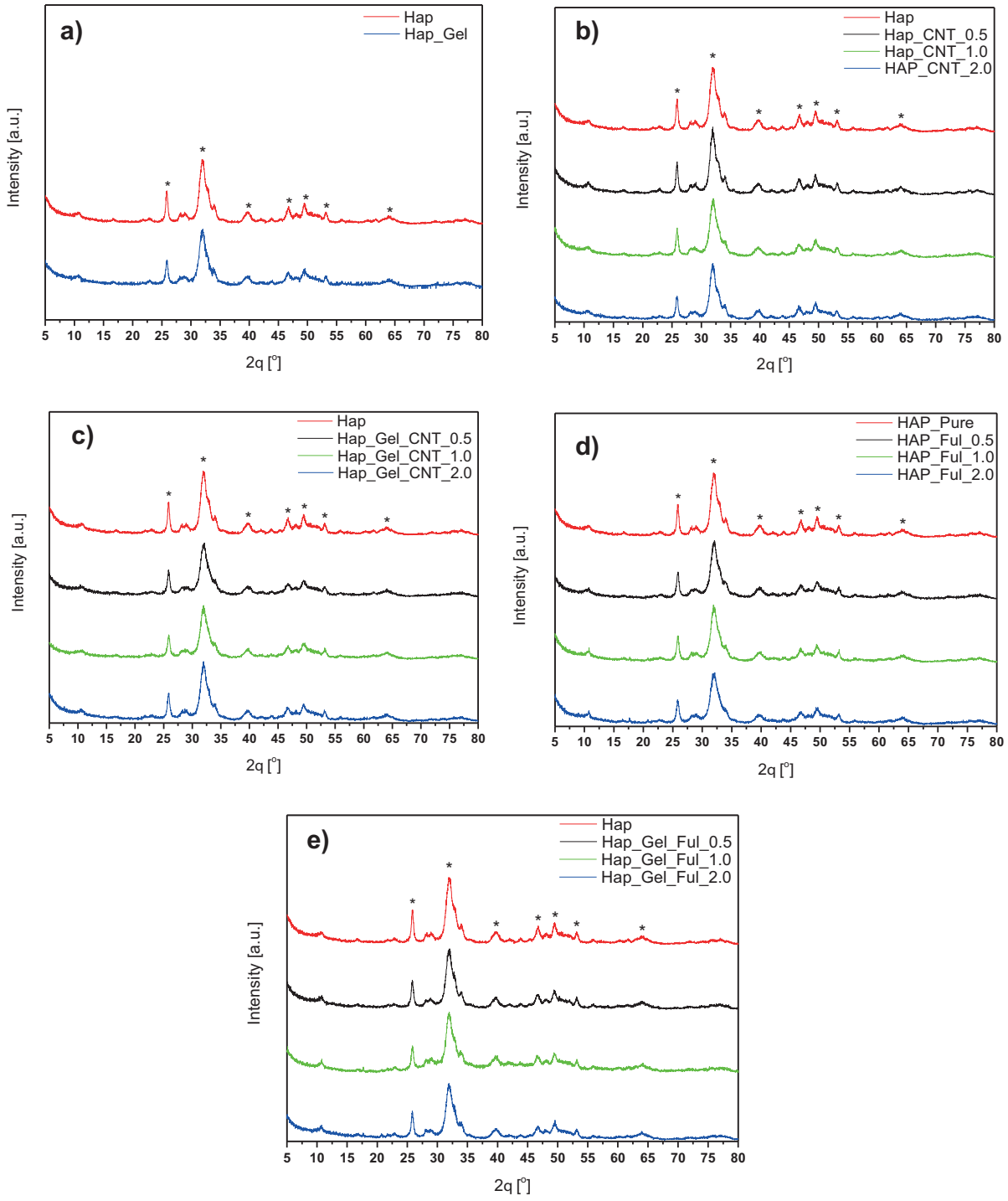

Figure 2. XRD patterns of (a) Hap_Gel, (b) Hap_fMWCNT, (c) Hap_Gel_fMWCNT, (d) Hap_Ful and (e) Hap_Gel_Ful NCs.

For Hap_Ful_2.0 and Hap_Gel_Ful_2.0, no obvious differences related to pure Hap were noted (Figures 3e and 3f). The twin bands at 2341 and 2361 cm^{-1} were the characteristic bands for aliphatic carbons.[26]

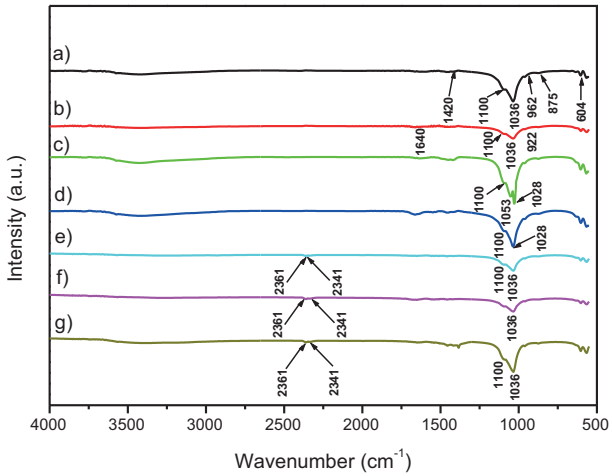

Figure 3. FT-IR spectra of (a) pure Hap, (b) Hap_Gel, (c) Hap-fMWCNT_2.0, (d) Hap_Gel_fMWCNT_2.0, (e) Hap_Ful_2.0, (f) Hap_Gel_Ful_2.0, (g) Hap_GO_2.0 NCs.

For Hap_GO_2.0, the band at 1385 cm^{-1} was attributed to C=C bonds, indicating the presence of GO and the twin bands at 2341 and 2361 cm^{-1} were also the characteristic bands for aliphatic carbons (Figure 3g).[26] Thus, the FT-IR spectra showed the presence of additives (CNT, Ful, and GO) in NCs and no significant changes in their characteristic bands.

2.5. Thermal analysis

The TG/DTA analysis of Hap-based NCs containing 2 wt.% nanocarbon additives (CNT, Ful, and GO) is presented in Figure 4. The quantity of additive (nanocarbon compound) was measured and compared to the theoretical value (2.0 wt.%).

For pure Hap, weight loss in the range of 30–110 °C, attributed to physically and weak chemically bound water (moisture), is associated on the TG curve with a weight loss of 4% (Figure 4a). All dissociation products disappear as gas between 170 and 210 °C and a small percentage of water is released from the pores until 500 °C (small exothermic peak at 340 °C). The thermal decomposition of calcium phosphates takes place between 550 and 800 °C, while between 700 and 1000 °C the last adsorbed water is released, indicating the decomposition of Hap to CaO and $Ca_3(PO_4)_2$.[27]

For Hap_Gel, the exothermic effect at 235–430 °C with the maximum at 335 °C is attributed to the decomposition of Gel.[28] A total weight loss of 15.86% was observed (Figure 4b); from 10 wt.% Gel only approximately 6 wt.% was detected, the other part probably being lost during the washing process.

Similar to pure Hap, for Hap_fMWCNT, a similar weight loss (3.5%) was observed in the range of 30–110 °C (Figure 4c). The sharp exothermic peak at 525 °C was attributed to fMWCNT decomposition. Similar results were obtained in our previous work.[22,29] Mahajan et al. reported that, in air, MWCNTs are thermally stable up to 420 °C (no phase change or oxidation reaction), when they start to degrade due to the combustion of the remaining amorphous carbon. The TEM studies confirmed that the walls of MWCNTs start to degrade, forming bundles, at 500 °C.[30] According to Boom et al., the oxidation of MWCNTs occurred at 630 °C.[31] The experimental weight percentage of CNT (2.0%) was in total accordance with the theoretical value.

Similar behavior to Hap_Gel and Hap_fMWCNT was observed for Hap_fMWCNT_Gel, accompanied

by a 2.0 weight loss corresponding to CNT in total agreement with the theoretical value (Figure 4d). The two exothermic peaks at 328 and 533 °C correspond to the decomposition of Gel and CNT.

For Hap_Ful, the sharp exothermic peak at 550 °C is assigned to the decomposition of Ful (Figure 4e).[32] A total weight percentage of 2.0 wt.% Ful was detected, in total accordance with the theoretical value.

For Hap_Gel_Ful_2.0, the peaks at 335 and 556 °C were attributed to the decomposition of Gel (similar to Hap_Gel) and the decomposition of Ful (similar to Hap_Ful), respectively (Figure 4f). A total weight percentage of 2.0 wt.% Ful was measured, in total agreement with the theoretical value.

The Hap_GO seems to be less sensitive to water adsorption from air compared to pure Hap or the water is more strongly bonded and it is released only at 110–500 °C (Figure 4g). The sharp exothermic peak at 344 °C was attributed to GO decomposition, while the exothermic peak at 640 °C was designated to combustion of the decomposition product of GO.[33] A total amount of 1.9 wt.% GO was detected, slightly lower than the theoretical value, probably due to the overlap with other peaks.

2.6. Compression test

A test method was developed for the determination of the compressive properties of Hap-based NCs.

2.6.1. Compression curve

The pure Hap was uniaxially pressed in a cylindrical die with a diameter of 6 mm. The optimum compression pressure was determined using the experimental compression curve (Figure 5): the test samples were produced using 0.200 g of material compressed at 300, 400, 500, 750, 1000, and 1500 MPa. Subsequently, the samples were weighed and measured to determine their density (the theoretical density of Hap is 3.16 kg/dm^3).[34]

2.6.2. Determination of uniaxial compression parameters

The stratification, overall strength, and consistency of samples prepared at different pressures were investigated by light microscopy. Starting at 750 MPa, the samples exhibited low visible stratification and high compressive strength and consistency. However, the samples pressed at 750 MPa did not provide a sufficient degree of consistency in the testing results; therefore, the compression pressure used was set at 1000 MPa. At the edges, a crown form about 100 µm high was observed. To eliminate this crown, a pre-pressure of 4–8 N was used, taking into account that this parameter is an important factor for the direction coefficient of the compression test curve (Figure 6).

The feed rate was determined empirically; a high feed rate gives inaccurate results concerning the brittleness of samples due to the low shock resistance. The best results were provided for the following feed rates (mm/min): 1 (initial), 0.5 (middle), and 0.2 (final).

During the compression tests of pure Hap the material broke into smaller pieces that spread around the test block (Figure 7a), while in the case of NCs containing CNTs (Figure 7b) the splinters remained closer to the samples. The Hap_Ful NCs were also riven into small scattered pieces (Figure 7c), like in the case of pure Hap. The NCs containing GO (Figure 7d) exhibit similar behavior to NCs containing CNTs.

2.6.3. Compression tests

The results of the compression tests are shown in Figure 8.

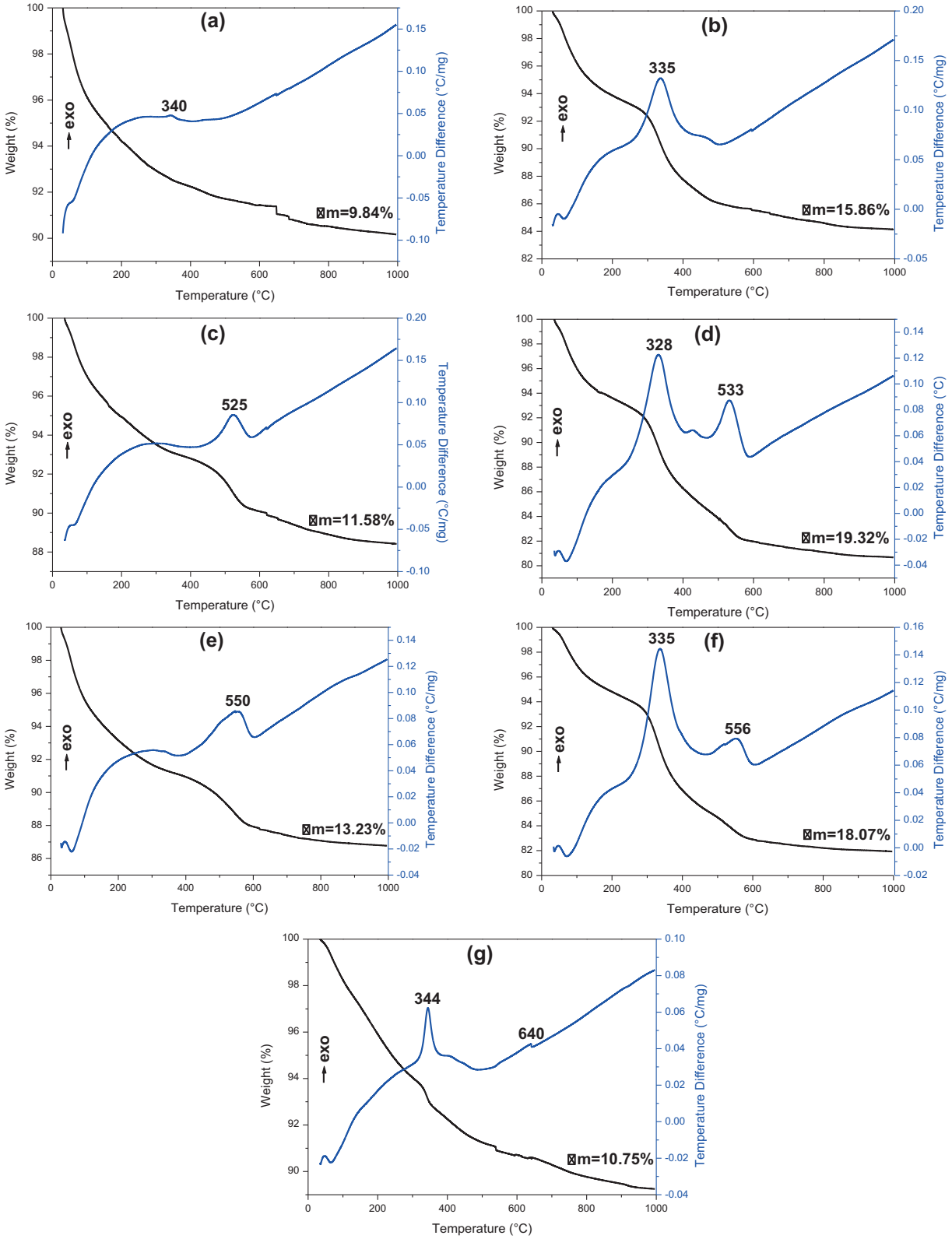

Figure 4. TG (black)/DTA (blue) plot of (a) pure Hap, (b) Hap_Gel, (c) Hap_fMWCNT, (d) Hap_Gel_fMWCNT, (e) Hap_Ful, (f) Hap_Gel_Ful, and (g) Hap_GO NCs.

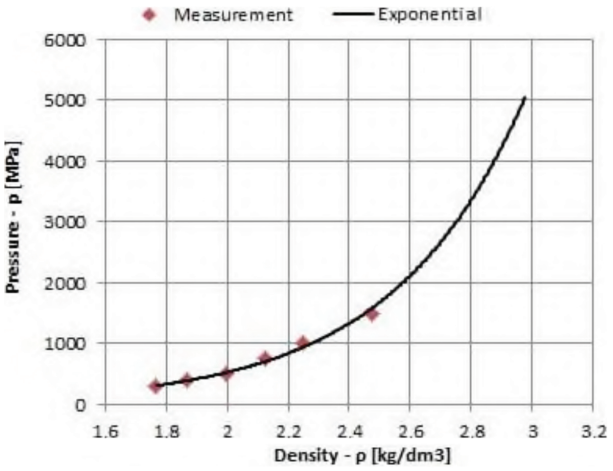

Figure 5. Experimental compression curve of pure Hap specimens at different uniaxial pressures.

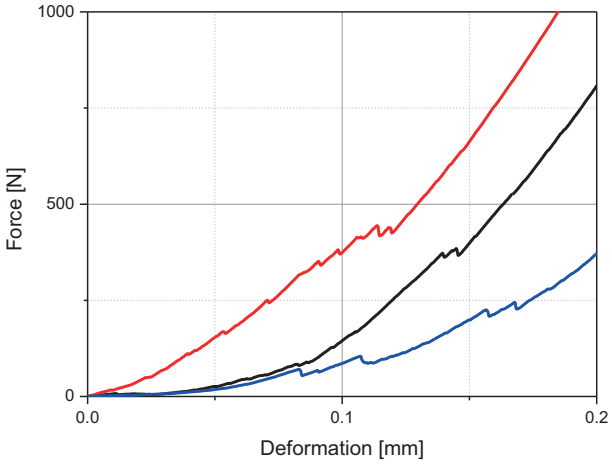

Figure 6. Difference in curve direction coefficient at different pre-pressures.

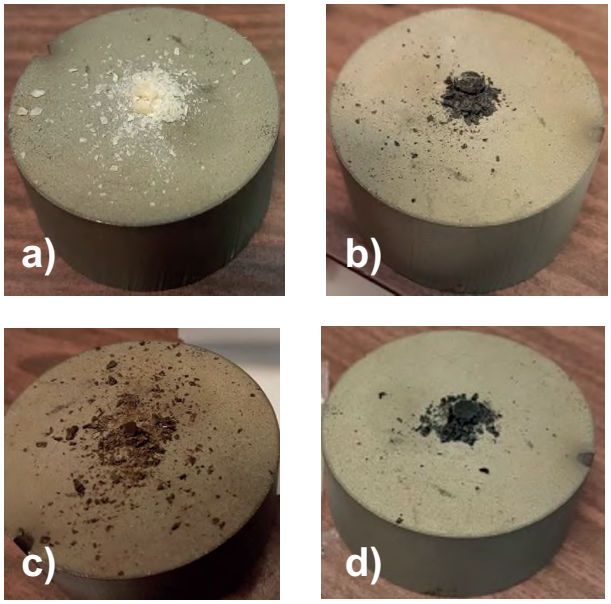

Figure 7. Samples after destruction: (a) pure_Hap, (b) HAP_fMWCNT_1.0, (c) Hap_Ful_1.0, (d) Hap_GO_1.0 NCs.

A compressive strength of 106 MPa was observed for pure Hap. This value is comparable with the compressive strength of cortical bone (100–230 MPa) and cancellous bone (2–12 MPa).[35] The addition of Gel considerably improved the mechanical properties, the compressive strength increasing 25.5% compared to pure Hap. A possible explanation is the 3D network structure of Gel.[36]

In contrast, the addition of fMWCNTs had a negative effect on the mechanical properties: the compressive strength of Hap_fMWCNT_0.5 and Hap_fMWCNT_2.0 NCs decreased 14.2% and 34.0% compared to pure Hap; Hap_fMWCNT_1.0 was an exception (+3.7%). A possible explanation is the smaller crystallite size (25.0 nm, see Table 1), which results in a better stacking of the nanoparticles during the uniaxial compressing and a higher density and strength.

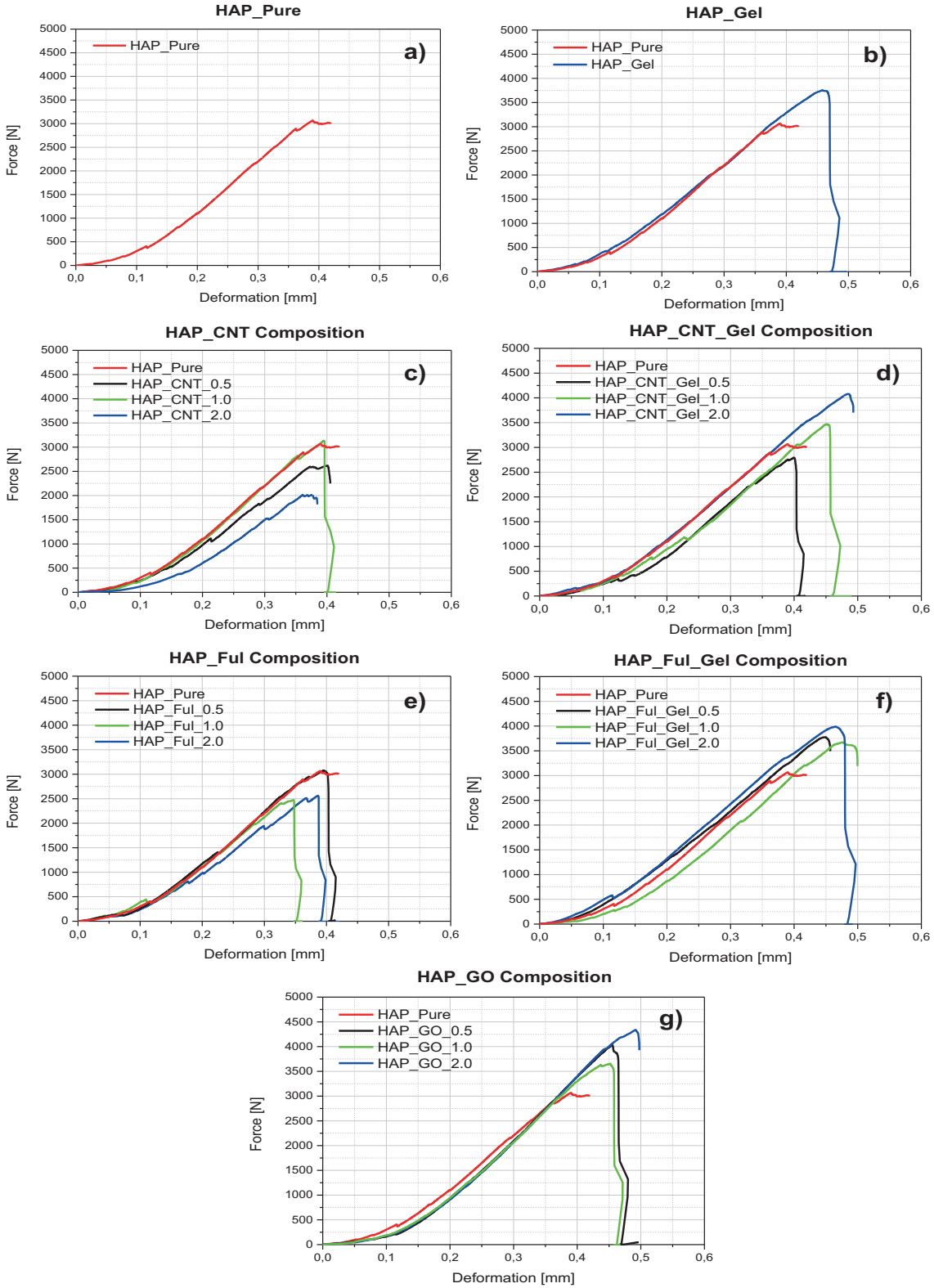

Figure 8. Compression curve of (a) pure Hap, (b) Hap_Gel, (c) Hap_fMWCNT, (d) Hap_Gel_fMWCNT, (e) Hap_Ful, (f) Hap_Gel_Ful NCs, and (g) Hap_GO NCs.

The mixed addition (fMWCNT and Gel) had a positive effect on the mechanical properties of Hap_Gel_fMWCNT_1.0 and Hap_Gel_fMWCNT_2.0 NCs (+17.0% and +36.8% compared to pure Hap). The negative values (–13.2%) of Hap_Gel_fMWCNT_0.5 can be explained by the larger crystallite size (27.0 nm), which yields a lower compression strength.[37]

The addition of Ful to Hap had a negative effect on the mechanical properties of the samples: –0.1%, –26.9%, and –27.4% compared to pure Hap. A possible explanation is that the smaller, buckyball-shaped Ful particles form points of stress concentration in the sample material, resulting in a sudden and explosive break at breaking force.

The mixed addition (Ful and Gel) had a positive effect on the mechanical properties of NCs, with Gel acting as an adhesive material between particles.[17] The increase in Ful content resulted in higher compressive strength: +24.5% (Hap_Gel_Ful_0.5), +23.6% (Hap_Gel_Ful_1.0), and +33.0% (Hap_Gel_Ful_2.0) compared to pure Hap. The results obtained indicate that the positive effect of Gel dominates the negative effect of Ful particles, leading to increasing compressive strength.

The addition of GO had a significant positive effect on the mechanical properties/compressive strength, as follows: +33.0% (Hap_Gel_Ful_0.5), +19.8% (Hap_Gel_Ful_1.0), and +43.4% (Hap_Gel_Ful_2.0); some possible explanations could be the strength of covalent bonds between carbon atoms, the great tensile strength, and the high surface area to volume ratio of GO.[38] This suggests that GO nanosheets are capable of absorbing high amounts of strain energy, stopping crack propagation, and functioning as a "slipping mat" between the stacked Hap nanoparticles, resulting in a higher compressive strength. Similar results were obtained for GO-Hap composites obtained by biomimetic in situ mineralization, which exhibited optimal mechanical properties (tensile strength and Young's modulus) and biocompatibility to mimic natural bone in both structure and function.[38]

It can be concluded that the addition of Gel improves the compressive strength of Hap-based NCs, better than the addition of fMWCNTs or Ful. The highest compression strength was achieved for GO. The different effect of GO and fMWCNTs on compressive strength is due to their different structures. Similar to graphene, GO has a two-dimensional crystal structure formed by a planar monolayer of carbon atoms arranged in a hexagonal lattice. The GO plans reduce the stresses caused by compression, resulting in a toughening mechanism of GO-based materials such as crack bridging, pull-out, crack deflection, and crack tip shielding.[39] Furthermore, in the case of the uniaxial compression test of a cylindrical sample, the applied axial stress results in a circumferential stress component acting as transverse tensile stress on the sample's wall. This circumferential stress component seems to be reduced in GO plans, while fMWCNTs seem to be less effective in reducing stress and crack propagation.[40]

2.7. Conclusions

In order to improve the mechanical properties of Hap-based materials, different additives (Gel and nanocarbon compounds with different morphologies and high specific surface) and content (10 wt.% Gel related to the Hap quantity and 0.5, 1.0, and 2.0 wt.% nanocarbon compounds) were considered. The NCs were prepared using an in-house innovation, "SmartBox", based on IoT, resulting in high reproducibility and precise and easy control of the reaction parameters. Their physicochemical and mechanical properties (compression strength) were investigated. XRD and FT-IR indicated the presence of additives in the Hap-based samples. The addition of Gel considerably improved the mechanical properties of Hap-based NCs, due to the adhesive, high elastic, and

plastic deformation characteristics of Gel compared to the breakable Hap nanoparticles. GO also had a positive effect on the compressive strength, GO sheets acting as slipping mats between the layers of Hap nanoparticles, absorbing high amounts of energy and stopping crack propagation. The mixed addition of fMWCNTs and Ful decreased, while the mixed addition of CNTs/Ful and Gel increased the compressive strength of NCs. It can be concluded that the morphology of nanocarbon additives has an obvious influence on the mechanical properties of Hap-based NCs. On the other hand, the smaller crystallite size and the possibility to create a network among the particles (like in the case of Gel addition) have positive effects on the compressive strength of Hap-based NCs.

3. Experimental

3.1. Materials

The fMWCNTs (characteristics: $>95\%$ purity, average external diameter of <8 nm, length of 30 µm, surface area of 500–700 m^2/g, and 3.86 wt.% carboxylate groups), GO (characteristics: $>99\%$ purity, 1–2 layers, thickness of 0.55–3.74 nm, diameter of 0.5–3 µm, and specific surface area of 500–1000 m^2/g), and Ful (characteristics: $>99.5\%$ purity and diameter of 0.7–1.1 nm) were purchased from TimesNano, Chengdu Organic Chemicals Co. Ltd., China. The bovine Gel type B (Mw = 20,000–25,000) and all other reagents were of analytical grade (Merck, Germany) and used as received without further purification.

3.2. Synthesis of hydroxyapatite

Hap was prepared by precipitation using $Ca(NO_3)_2 \cdot 4H_2O$ as a source of Ca^{2+} and $(NH_4)_2HPO_4$ as a source of PO_4^{3-}.[41] An aqueous solution of 0.09 mol/L $(NH_4)_2HPO_4$ was added dropwise with a feed rate of 25 mL/min, using a peristaltic pump, into a stirred aqueous solution of 0.15 mol/L $Ca(NO_3)_2 \cdot 4H_2O$, at room temperature. The pH was adjusted to 11 by adding 25% ammonia solution under constant stirring at room temperature. The suspension was matured for 22 h, filtered, and washed and the resulting precipitate was dried at 110 °C.

3.3. Synthesis of Hap-based NCs

The Hap-based NCs (Table 2) were prepared by precipitation in a similar way to the synthesis of pure Hap. The appropriate quantities of additives were added to a 0.5 mol L^{-1} $Ca(NO_3)_2$ solution; the pH was adjusted to 11 by adding a 25% ammonia solution, under constant stirring, at room temperature. After the pH adjustment, a $(NH_4)_2HPO_4$ 0.3 mol L^{-1} solution was added dropwise, with a feed rate of 25 mL/min, using a peristaltic pump, under magnetic stirring, at room temperature, for 22 h. The resulting precipitate was filtered, washed with distilled water, and dried at 110 °C.

The best amount of nanocarbon in composite materials can be defined as the amount that causes an increase in some of the useful materials' properties to the highest level.[42] Moreover, the difference between macromolecules or nanomaterials used as additives should be considered, nanomaterials exhibiting their effect on final properties even in lower amounts, due their high specific surface area.[43] The use of high amounts of additives (e.g., >
10%) with large specific surface area, such as nanocarbon compounds (theoretical surface area of graphene $\sim$ 2600 m^2/g, CNT $\sim$ 1000 m^2/g),[29,44] leads to difficulties in the preparation (large volume and low quantity of additives) and makes no sense since the use of small quantities of nanocarbon compounds (0.5, 1.0, and 2.0

wt.%. GO, fMWCNT, and Ful) has the same effect on the physicochemical and mechanical properties of final NCs.

Table 2. Synthesis route for Hap and Hap-based NCs.

No.		fMWCNTs (wt.%)	GO (wt.%)	Ful (wt.%)	Gel (wt.%)	Samples
z						
1	Hap	-	-	-	-	Pure Hap
2		-	-	-	10	Hap_Gel
3		0.5	-	-	-	Hap_fMWCNT_0.5
4		1.0	-	-	-	Hap_fMWCNT_1.0
5		2.0	-	-	-	Hap_fMWCNT_2.0
6		0.5	-	-	10	Hap_Gel-fMWCNT_0.5
7		1.0	-	-	10	Hap_Gel-fMWCNT_1.0
8		2.0	-	-	10	Hap_Gel_fMWCNT_2.0
9		-	-	0.5	-	Hap_Ful_0.5
10		-	-	1.0	-	Hap_Ful_1.0
11		-	-	2.0	-	Hap_Ful_2.0
12		-	-	0.5	10	Hap_Gel_Ful_0.5
13		-	-	1.0	10	Hap_Gel_Ful_1.0
14		-	-	2.0	10	Hap_Gel_Ful_2.0
15		-	0.5	-	-	Hap-GO_0.5
16		-	1.0	-	-	Hap-GO_1.0
17		-	2.0	-	-	Hap_GO_2.0

3.4. The Internet of things

The NCs were prepared using an in-house "IoT-Smartbox" equipped with temperature sensor, heating element, pH-meter, and peristaltic pump and connected to the Internet to give anytime/anywhere monitoring and control of the process parameters (pH and temperature) and, in terms of safety, it automatically switches off if the critical temperature is reached or sends an alert message through SMS and email (in a "safe zone"). The process parameters (pH and temperature) were chosen due to their influence on the obtained material properties such as phase composition and particle size. Furthermore, "IoT-Smartbox" offers good reproducibility and the possibility to track the history of the process (Figure 9).

3.5. Characterization

The particle size distribution of NCs was measured in suspensions using a micro- and nanoparticle analyzer SALD-7101 (Shimadzu, Japan). The morphology of NCs was observed by a H7650 transmission electron microscope (TEM) (Hitachi, Japan). XRD analysis was performed at room temperature, using a D8 ADVANCE diffractometer (Bruker, Germany), operating at 40 kV and 40 mA with CuKα radiation ($\lambda = 1.54060$ Å). The

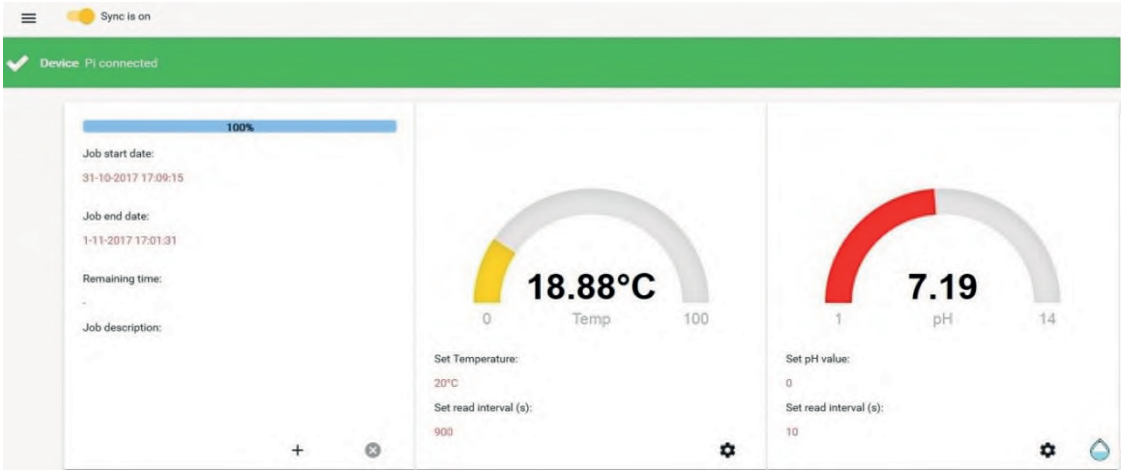

Figure 9. Screenshot of the IoT Internet portal.

average crystallite size was calculated using the Scherrer Eq. (1).

$$\lambda\beta\theta D_{h\,k\,l}=\frac{0.9}{\cos}, \tag{1}$$

where D is crystallite size, β is the broadening of full width at half the maximum intensity (FWHM), θ is the Bragg angle, and λ is the X-ray wavelength.[29]

The FT-IR spectra were recorded using a Bruker Vektor 22 (USA) FT-IR spectrometer. The thermogravimetry (TG) and differential thermal analysis (DTA) measurements were carried out with a TA Instrument SDT Q600 (USA), in an air atmosphere flow rate of 25 mL/min at a heating rate of 10 °C/min, in the temperature range from 30 to 1000 °C, using alumina crucibles. The compression tests were performed using a Z005 universal testing machine (Zwick-Roell, Germany).

Acknowledgments

This work was supported by the Sectorial Operational Program "Increase of Economic Competitiveness" Priority Axis II, Project Number 1887, INOVA-OPTIMA, code SMIS-CSNR 49164, and a mobility grant from the Romanian Ministry of Research and Innovation, CNCS-UEFISCDI, project number PN-III-P1-1.1-MC-2018-0816, within PNCDI III.

References

1. Zhou, H.; Lee J. *Acta Biomater.* **2011**, *7*, 2769-2781.
2. Radha, G.; Venkatesan, B.; Vellaichamy, A; Balakumar S. *Ceram. Int.* **2018**, *44*, 8777-8787.
3. Ong, Y. T.; Ahmad, A. L.; Zein, S.H.S.; Tan, S. H. *Brazil. J. Chem. Engineer.* **2010**, *27*, 227-242.
4. White, A. A.; Best, S. M.; Kinloch, I. A. *Int. J. Appl. Ceram. Tec.* **2007**, *4*, 1-13.
5. Chen, Y.; Zhang, T. H., Gan, C. H.; Yu, G. *Carbon* **2007**, *45*, 998-1004.
6. Costanda, S.; Stan, M. S.; Ciobanu, C. S.; Motelica-Heino, M.; Guegan, R.; Lafdi, K.; Dinischiotu, A.; Predoi, A. *J. Nanomater.* **2016**, Article ID 3941501, 10 pages.
7. Lahiri, D.; Singh, V., Keshri, A. K.; Seal, S. Agarwal A., *Carbon* **2010**, *48*, 3103-3120.

8. Fang, L.; Leng, Y.; Gao P. *Biomaterials* **2006**, *27*, 3701-3707.
9. Ramires, P.; Romito, A.; Cosentino, F.; Milella, E. *Biomaterials* **2001**, *22*, 1467-1474.
10. Abden, M. J.; Afroze, J. D.; Alam, M. S.; Bahadur, N. M. *Mater. Sci. Eng. C - Mater.* **2016**, *67*, 418-424.
11. Bhattacharya, K.; Mukherjee, S. P.; Gallud, A.; Buckert, S.C.; Bistarelli, S.; Belucci, S.; Bottini, M.; Star, A.; Fadeel B. *Nanomed. Nanotechnol.* **2016**, *12*, 333-351.
12. Zhao, X.; Chen, X.; Zhang, L.; Liu, Q.; Wang, Y.; Zhang, W.; Zheng, J. *Coatings* **2018**, *8*, 357-369.
13. Mukherjeea, S.; Kundub, B.; Senc, S; Chandad, A. *Ceram. Int.* **2014**, *40*, 5635-5643.
14. Le, H.; Natesan, K.; Pranti-Haran, S.; *J. Adv. Cer.* **2015**, *4*, 237-243.
15. Chao, S. C.; Wang, M. J.; Pai, N. S.; Yen, S. K., *Mat. Sci. Eng. C-Mater.* **2015**, *57*, 113-122.
16. Pek, Y. S.; Gao, S.; Arshad, M. S. M.; Leck, K. J.; Ying, J. Y. *Biomaterials* **2008**, *29*, 4300-4305.
17. Yanovska, .; Kuznetsov, V.; Stanislavov, A.; Husak, .; Pogorielov, .; Starikov, V.; Bolshanina, S.; Danilchenko, S. *Mater. Chem. Phys.* **2016**, *183*, 93-100.
18. Gil, D.; Ferrandez, A.; Mora-Mora, H.; Peral, J. *Sensors (Basel)* **2016**, *16*, 1069-1092.
19. Ley, S. V.; Fitzpatrick, D. E.; Ingham, R. J.; Nikbin, N. *Beilstein Magazine* **2015**, *1*, No. 2.
20. Ding, D.; Yu T.; Zhang, W.; Liu, W.; Huang, Y. *J. Nanomater.* **2015**, *Article ID 628405*, 6 pages.
21. Li, H.; Song, X.; Li, B.; Kang, J.; Liang, C.; Wang, H.; Yu, Z.; Qiao Z. *Mat. Sci. Eng. C - Mater.* **2017**, *77*, 1078-1087.
22. Barabas, R.; Cziko, M.; Dekany, I.; Bizo, L.; Bogya, E. S. *Chem. Pap.* **2013**, *67*, 1414-1423.
23. Rezakhani, A.; Kashani Motlagh, M. M. *Int. J. Phys. Sci.* **2012**, *7*, 2768-2774.
24. Yadav, S. K.; Bera, T.; Saxena, P. S.; Maurya, A. K.; Garbyal, R. S.; Vajtai, R; Ramachandrarao, P.; Srivastava, A. *J. Biomed. Mater. Res. A* **2010**, *93*, 886-924.
25. Mukherjee, S.; Kundu, B.; Chanda, A.; Sen S. *Ceram. Int.* **2015**, *41*, 3766-3774.
26. Stuart, B. H. *Infrared Spectroscopy: Fundamentals and Applications*; Wiley: Hoboken, NJ, USA, 2004.
27. Berzina-Cimdina L.; Borodajenko N. In: *Infrared Spectroscopy - Materials Science, Engineering and Technology*; Theophanides, T., editor. InTech: Rijeka, Croatia, 2012.
28. Chuaynukul, K.; Prodpran, T.; Benjakul S. *Res. J. Chem. Environ.* **2014**, *2*, 1-9.
29. Barabas, R.; Katona, G.; Bogya, E. S.; Diudea, M. V.; Szentes, A.; Zsirke, B.; Kovacs, J.; Kekedy-Nagy, L.; Cziko, M. *Ceram. Int.* **2015**, *41*, 12717-12727.
30. Mahajan, A.; Kingon, A.; Kukovecz, A.; Konya, Z.; Vilarinho, P. M. *Mater. Lett.* **2013**, *90*, 165-168.
31. Bom, D.; Andrews, R.; Jacques, D; Anthony, J.; Chan, B.; Meier, M. S.; Selegue, J. P. *Nano Lett.* **2002**, *2*, 615-619.
32. Nali, N.; Chipara, D.; Lozano, K.; Hinthorne, J. Chipara M. *Appl. Surf. Sci.* **2017**, *421*, 220-227.
33. Najafi, F.; Rajabi, M. *Int. Nano Lett.* **2015**, *5*, 187-190.
34. Kothapallia, C.; Wei, M.; Vasilieva, A.; Shaw, M. T. *Acta Mater.* **2004**, *52*, 5655-5663.
35. Hutmacher, D. W.; Schantz, J. T.; Lam, C. X. F.; Tan, K. C.; Lim, T. C. *J. Tissue Eng. Regen. Med.* **2007**, *1*, 245-260.
36. Barabas, R.; Rigo, M.; Ebiszne-Bodogh, M.; Moisa, C.; Cadar, O. *Stud. U. Babes-Bol. Che.* **2018**, *3*, 137-154.
37. Dong, X. H.; Hong, X. T.; Chen, F.; Sang, B. R.; Yu, W.; Zhang, X. P. *Mater. Des.* **2014**, *64*, 400-406.
38. Li, Y; Liu, C.; Zhjai, H.; Zhu, G.; Pan, H.; Xu, X.; Tang, R. *RSC Adv.* **2014**, *4*, 25398-25403.
39. Shin, S. R.; Li, Y. C.; Jang, H. L.; Khoshakhlagh, P.; Akbari, M.; Nasajpour, A.; Zhang, Y. S.; Tamayol, A.; Khademhosseini, A. *Adv. Drug Deliv.* **2016**, *105*, 255-274.
40. Hannora, A. E.; Ataya, S. *J. Alloy. Compd.* **2016**, *658*, 222-233.

41. Dejeu, V. R.; Barabas, R.; Cormos, A. M.; Sara, B. E.; Agachi P. S. *Stud. U. Babes-Bol. Che.* **2010**, *45*, 363-373.
42. Vahedi, A. F.; Shahverdi, H. R.; Shokrieh, M. M.; Esmkhani, M. *New Carbon Mater.* **2014**, *29*, 419-425.
43. Khan, I.; Saeed, K.; Khan, I. *Arab. J. Chem.* **2017**, in press.
44. Ramakrishna Matte, H. S. S.; Subrahmanyam, K. S.; Rao, C. N. R. *Nanomater. Nanotechnol.* **2011**, *1*, 3-13.